ELSEVIER

Contents lists available at ScienceDirect

# Journal of Materials Research and Technology

journal homepage: www.elsevier.com/locate/jmrt





# Mechanical behavior of material removal under various rake angle diamond tool ultra-precision cutting of titanium alloy

Lingyi Sun<sup>a</sup>, Xin Cui<sup>a,\*</sup>, Chunjin Wang<sup>b</sup>, Yanbin Zhang<sup>a,c</sup>, Changhe Li<sup>a,c</sup>

- a Key Lab of Industrial Fluid Energy Conservation and Pollution Control, Ministry of Education, Qingdao University of Technology, Qingdao, 266520, China
- b State Key Laboratory of Ultra-precision Machining Technology, Department of Industrial and Systems Engineering. The Hong Kong Polytechnic University, Hung Hom, Kowloon, Hong Kong
- <sup>c</sup> Qingdao University of Technology Intelligent and Sustainable Precision Manufacturing Institute, Qingdao, 266200, China

#### ARTICLE INFO

Keywords:
Titanium alloy
Material removal mechanism
Ultra-precision cutting
Nanolubricant

#### ABSTRACT

The titanium alloy TC4 (Ti-6Al-4V) is widely applied in ultra-precision machining of aerospace optical components due to its high specific strength and thermal resistance. Understanding their material removal mechanisms enables optimization of machining parameters, enhancement of surface quality, expansion of advanced processing techniques, and fulfillment of performance demands in high-end applications. However, existing predictive models often neglect the coupled effects of mechanical, frictional, and fluid dynamic fields, limiting their applicability and predictive accuracy. To address this, this study proposes a cutting force prediction framework integrating the Oxley cutting model with the Johnson–Cook constitutive model. By incorporating a dynamic friction coefficient, the model's accuracy is experimentally validated. The effects of different lubrication modes on surface defects are quantified, and the chip formation and scratch morphologies are examined. The results show that the model achieves an average prediction error of 8.23 %, with a minimum error of 3.54 %. Both rake angle and lubrication mode jointly affect the material removal behavior of TC4: a reduced rake angle intensifies plowing and fracture, whereas the nanolubricant minimum quantity lubrication (NMQL) mode effectively reduces scratch depth. This approach provides a theoretical foundation for understanding cutting force evolution in machining TC4 and serves as a reference for tool design and machining parameter selection.

#### Nomenclature

MQL	Minimum quantity lubrication	NMQL	Nanolubricant minimum quantity lubrication
$F_s$	Shear force	$ au_s$	Shear stress
$A_s$	Cross-sectional area of cutting layer	$A_c$	Cutting layer area
$a_p$	Depth of cut	f	Feed rate
v	Cutting speed	$\gamma_0, \phi$ ,	Rake angle, shear angle,
		β	friction angle
$V_c$	Chip flow velocity	$F_{fc}$	Friction force along the rake
			face
$F_c$	Main cutting force	$F_t$	Tangential force
F	Resultant cutting force	$F_p$	Vertical component of
		-	resultant cutting force
$F_{nc}$	Normal force on the rake face	Α	Initial yield stress
ε, έ,	Shear strain, shear strain rate,	В	Hardening modulus
$\dot{\varepsilon}_0$	reference shear strain rate		
C	Strain rate sensitivity coefficient	n	Strain hardening index
			(continued on next column)

<sup>(</sup>continued)

m	Temperature softening coefficient	T	Temperature of cutting zone
$T_r$	Ambient temperature	$T_m$	Material melting point

#### 1. Introduction

Titanium alloy, particularly TC4 (Ti-6Al-4V), is widely applied in aerospace, biomedical, and precision engineering industries due to its high specific strength, heat resistance, and corrosion resistance [1–3]. However, poor machinability, including low thermal conductivity, strong chemical reactivity with tools, and pronounced work hardening tendency, presents significant challenges in precision and ultra-precision machining [4–7]. Investigating the material removal mechanism is fundamental for addressing these challenges, as it supports innovation in processing technology, advances in tool design, and provides theoretical guidance for manufacturing high-performance

E-mail address: cxinxin5240@163.com (X. Cui).

#### https://doi.org/10.1016/j.jmrt.2025.07.225

<sup>\*</sup> Corresponding author.

components [8–14]. For example, Xu et al. [15] investigated the material removal mechanism of SiC fiber-reinforced Ti alloy matrix composites by proposing a laser-assisted grinding method. Wang and Qu [16] f analyzed the surface morphologies and composition at the groove end area to investigate the material removal mechanism in TC4 titanium alloy. Siva Surya [17] reported that the depth of cut is the most significant parameter influencing the material removal rate when turning Ti–6Al–4V using a Micromatic automated computer numerical control lathe.

The development of a cutting force model is essential for understanding the ultra-precision machining behavior of titanium alloys, enabling quantitative analysis of force responses and material removal mechanisms under varying cutting parameters [18-21]. Substantial research has been conducted in this area [22-25]. For instance, Ma et al. [26] proposed a cutting force prediction model for Ti-6Al-4V, considering friction at the tool-chip contact interface during ultrasonic longitudinal torsional vibration-assisted milling. The predicted dynamic milling force agreed well with measured values, with errors in the X and Y directions of 5.51 % and 10.23 %, respectively. Shen et al. [27] established Johnson-Cook constitutive models for TC17 titanium allov using parameter identification, showing that the model accurately predicts flow stress at high strain rates and across wide temperature ranges. Li et al. [28] refined the cutting force and chip breaking model for vibration-assisted drilling of Ti-6Al-4V, analyzing dynamic motion angle, parameter effects, and cutting strain during intermittent vibration-assisted machining.

In applications where surface integrity, dimensional accuracy, and tool wear control are critical, conventional machining strategies often fail to meet stringent requirements. To further reduce friction, minimum quantity lubrication (MQL) has been proposed [29-32]. MQL forms an oil film that facilitates rapid heat transfer, thus reducing thermal damage. Mohandas et al. [33] compared the effect of cutting speed on surface roughness of Ti-6Al-4V under soluble oil and MQL, finding a greater effect with MQL. In studies on titanium alloy Ti-5Al-2.5Sn, Shi et al. [34] found that supercritical carbon dioxide (scCO2)-oil based on MQL can address oil film rupture and insufficient wear reduction observed with MQL or scCO2 cooling alone. Sarma et al. [35] optimized the processing quality of Ti-6Al-4V under MQL by applying the Jaya algorithm and support vector regression modeling, resulting in improved surface roughness. Nanolubricant minimum quantity lubrication (NMQL) can further optimize friction due to the size effect of nanoparticles, which more effectively fill microscopic gaps between the tool and workpiece [36-39]. The stable lubricating film formed by NMQL can enhance friction behavior more efficiently than conventional MQL. For example, Biyik [40] produced equiaxed nanocrystalline Ag-ZnO composite powder (average particle size 1.077 μm) by ball milling with Y<sub>2</sub>O<sub>3</sub> doping, achieving fine, uniform dispersion of oxide in the silver matrix. In another study, Biyik [41] synthesized nanocrystalline Cu25Mo composite powder with particle size approximately 2.215 µm via extended ball milling. Both nanoparticles are promising candidates for improving the cooling efficiency and tribological performance of NMQL technology. Kim et al. [42] analyzed flow and heat transfer during Ti-6Al-4V milling using a hybrid NMQL and cryogenic nitrogen lubrication method, finding the hybrid approach preferable. Namlu et al. [43] investigated the efficiency of multi-axial ultrasonic vibration-assisted machining with hybrid NMQL for Ti-6Al-4V, concluding that it enhances machining efficiency.

Addressing the substantial challenges imposed by the thermomechanical properties and dynamic effects during grinding requires investigation into the mechanical behavior of material removal and the establishment of a grinding force model. Therefore, this study focuses on the material removal mechanism and cutting force behavior during the grinding of titanium alloy TC4 with a diamond tool, and develops a theoretical prediction framework based on the Oxley cutting model and the Johnson-Cook constitutive model. On this basis, the distribution law of cutting force and the mechanical response characteristics of the

material are systematically analyzed. Combined with analysis of friction behavior under different lubrication modes, a dynamic friction coefficient model for the cutting process is established. Corresponding grinding experiments are then designed and conducted. The theoretical model is validated against experimental results, and microscopic mechanisms, such as scratch depth and chip formation, are further explored.

# 2. Cutting mechanical behavior of titanium alloy with negative rake angle

## 2.1. Cutting force distribution

Understanding the material removal mechanism in metals is fundamental for developing a theoretical cutting force prediction model, which also governs chip formation. The Oxley model is a classic contact mechanics framework for analyzing the coupled behavior of heat, force, and material flow within the shear zone during metal cutting processes [44,45]. Compared with other shear models, it accounts for multiple variables, including tool rake angle, cutting speed, feed rate, and lubrication condition. The model enables accurate characterization of the thermal-force coupling process and effectively simulates the behavior of difficult-to-machine materials such as titanium alloys [46, 47]. By incorporating strain hardening, strain rate sensitivity, and thermal softening, the Oxley model balances theoretical rigor with computational efficiency, resulting in high predictive accuracy and enhanced applicability across a wide range of cutting conditions [48].

The force analysis for orthogonal cutting is depicted in Fig. 1. The resultant force acting on the chip can be decomposed into two sets of components: (i) the normal force  $F_{nc}$  perpendicular to the rake face and the frictional force  $(F_{fc})$  along the rake face, and (ii) the shear force  $(F_s)$  along the shear plane and the compressive force  $(F_p)$  normal to the shear plane. These force pairs form equilibrium states, with their vector sums equal in magnitude and opposite in direction. The resultant cutting force can further be resolved into two orthogonal components: the main cutting force  $(F_c)$  in the direction of tool motion and the tangential force  $(F_t)$  perpendicular to the cutting direction.

Assuming uniform shear stress on the primary shear plane and applying the Von Mises failure criterion, the shear force is given by:

$$A_{s} = \frac{A_{c}}{\sin \phi} = \frac{a_{p} \cdot f}{\sin \phi} \tag{1}$$

$$F_s = \tau_s A_s = \frac{\tau_s \cdot a_p \cdot f}{\sin \phi} \tag{2}$$

where  $F_s$  is the shear force.  $\tau_s$  is the shear stress on the shear plane.  $A_s$  is the cross-sectional area of cutting layer.  $A_c$  is the area of cutting layer.  $a_p$  is the depth of cut. f is the.  $\phi$  is the shear angle.

Based on the velocity vector distribution in Fig. 1:

$$V_c = \frac{\sin \phi}{\cos(\phi - \gamma_0)} V \tag{3}$$

where V is the cutting speed.  $V_c$  is the chip flow velocity.  $\gamma_0$  is the rake angle.

According to the geometric relationship between tool and chip in orthogonal cutting, the following can be established:

$$F = \frac{F_s}{\cos(\phi + \beta - \gamma_0)} \tag{4}$$

$$F_p = F_s \tan(\phi + \beta - \gamma_0) \tag{5}$$

$$F_{fc} = F \sin \beta = \frac{F_s \sin \beta}{\cos(\phi + \beta - \gamma_0)}$$
 (6)

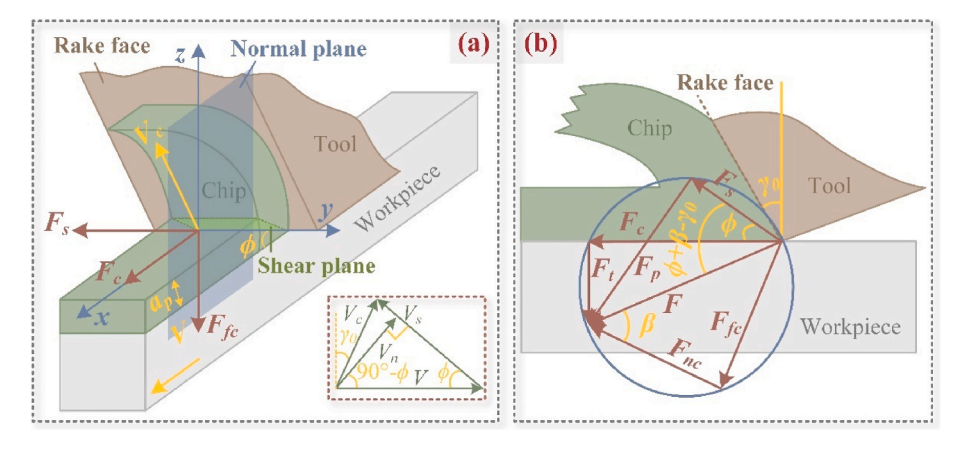


Fig. 1. Force analysis of orthogonal cutting: (a) Geometric model of orthogonal shear force; (b) Diagram of orthogonal cutting forces.

$$F_{nc} = F \cos \beta = \frac{F_s \cos \beta}{\cos(\phi + \beta - \gamma_0)}$$
 (7)

$$F_c = F\cos(\beta - \gamma_0) = \frac{F_s\cos(\beta - \gamma_0)}{\sin\phi\cos(\phi + \beta - \gamma_0)}$$
(8)

$$F_t = F\sin(\beta - \gamma_0) = \frac{F_s\sin(\beta - \gamma_0)}{\cos(\phi + \beta - \gamma_0)}$$
(9)

where  $F_c$  is the main cutting force.  $F_t$  is the tangential force. F is the resultant cutting force.  $F_p$  is the vertical component force of the resultant cutting force.  $F_{fc}$  is the friction force along the rake face.  $F_{nc}$  is the normal force on the rake face.  $\beta$  is the friction angle.

#### 2.2. Material controlling equation

The accuracy of cutting force prediction is strongly influenced by the material properties of the workpiece, making the development of an accurate flow stress model essential. The Johnson-Cook constitutive model is widely recognized for its ability to capture strain hardening, strain rate sensitivity, and thermal softening, thus reflecting the complex behavior of metals during grinding [49,50]. In this study, the Johnson-Cook model is employed to describe the dynamic mechanical response of TC4 under high temperature and high strain rate conditions:

$$\sigma = (A + B\varepsilon^{n}) \left[ 1 + C \ln \left( \frac{\dot{\varepsilon}}{\dot{\varepsilon}_{0}} \right) \right] \left[ 1 - \left( \frac{T - T_{r}}{T_{m} - T_{r}} \right)^{m} \right]$$
 (10)

where e is the shear strain.  $\dot{e}$  is the shear strain rate.  $\dot{e_0}$  is the reference shear strain rate. A is the initial yield stress, B is the hardening modulus, C is the strain rate sensitivity coefficient, n is the strain hardening exponent, m is the thermal softening exponent, T is the cutting zone temperature,  $T_r$  is the ambient temperature, and  $T_m$  is the material melting point.

The shear angle  $(\phi)$  is typically affected by elastic-plastic deformation on the shear plane and by severe friction at the rake face, and can be calculated by Eq. (11):

$$\phi = \arctan \frac{\cos \gamma_0}{\zeta - \sin \gamma_0} \tag{11}$$

where  $\zeta$  is the chip deformation coefficient. For titanium alloy cutting,  $\zeta$  is about 1.

The friction coefficient  $(\mu)$  between workpiece and tool is given by Eq. (12):

$$\mu = \tan \beta = \frac{F_t \cos \gamma_0 + F_c \sin \gamma_0}{F_c \cos \gamma_0 - F_t \sin \gamma_0}$$
(12)

Eq. (12) rigorously decouples the interfacial friction from measured

resultant forces based on orthogonal force resolution, thereby avoiding dependence on shear angle estimation. Unlike materials such as aluminum, which exhibit stable shear localization, TC4 displays dynamic shear band migration during machining, making this approach advantageous.

Due to the nonlinear variation in cutting characteristics, lubrication mode, and cutting force, friction coefficients are more accurately determined through experimental data rather than direct substitution of theoretical values. Fig. 2 presents the variation in friction coefficient with different lubrication modes. As the rake angle decreases, the pressure between the tool and workpiece increases, resulting in a higher friction coefficient. Under dry cutting, the absence of lubrication leads to greater contact damping and the largest increase in friction coefficient. For instance, decreasing the rake angle from  $0^{\circ}$  to  $-30^{\circ}$  results in a 45.2 % increase in friction coefficient under dry cutting, and a 35.9 % increase under NMQL. To control for external factors, data at a rake angle of  $0^{\circ}$  are compared. Averaged across multiple experiments, the friction coefficient values are 0.575 (dry), 0.484 (MQL), and 0.387 (NMQL). The Johnson-Cook model parameters and the physical and mechanical properties of TC4 are presented in Tables 1 and 2, respectively.

#### 3. Experimental validation and result analysis

#### 3.1. Experimental setup

The experimental setup is illustrated in Fig. 3. As depicted in Fig. 3 (a), all machining procedures were conducted on a four-axis ultra-precision lathe (Moore Nanotech 350 FG, Moore Nanotechnology Systems, USA). This system integrates Fast Tool Servo capability with hydrostatic-bearing stages along the X, Z, and C axes, as well as a high-stiffness B axis. Cutting forces in two directions were measured using a Kistler

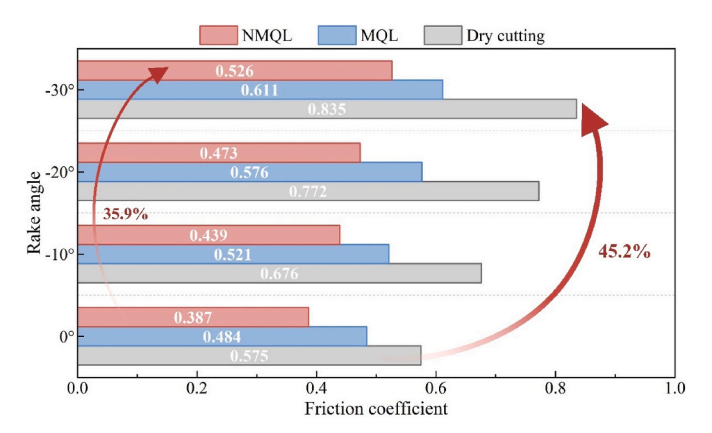


Fig. 2. Changes in friction coefficient under different lubrication modes.

Table 1
Johnson-Cook parameters of TC4 [51].

A (MPa)	B (MPa)	С	n	m	$\dot{\varepsilon}_0$ (s <sup>-1</sup> )	$T_m$ (°C)	$T_r$ (°C)
782	498	0.028	0.28	1	0.00001	1650	20

**Table 2** Physical and mechanical property parameters of TC4 [51].

Elastic modulus (GPa)	Thermal conductivity (W/ (m°C))	Specific heat capacity (J/ (kg°C))	Density (kg/m3)	Poisson's ratio	
136	7.6	611	4500	0.34	

9256C dynamometer, with sensitivity set to 24.63 and a natural frequency of 5.1 kHz. Data acquisition was performed at a sampling rate of 50 kHz. The Dynoware software (Kistler) was employed for synchronized analysis and visualization of the cutting force data. As shown in Fig. 3(f), an external lubrication device provided coolant delivery. As depicted in Fig. 3(g), chip morphology was examined using a Hitachi HT3030 scanning electron microscope (SEM). Microstructural characterization was performed with a field-emission SEM (Hitachi TM3000 Desk-top SEM), achieving a resolution of 30 nm.

Tool geometry is presented in Fig. 3(c). The single-crystal diamond tool, sourced from Contour Fine Tooling LLC (USA), features a Type IIa crystal structure with <110> orientation, a nose radius of 1 mm, and a clearance angle of  $15^\circ$ . The Mohs hardness of the diamond tool is 10. As shown in Fig. 3(d), TC4 titanium alloy specimens with dimensions D12  $\times$  2 mm were selected as the workpiece material. The sample was secured on fixture 1 using screws, with the configuration depicted in

Fig. 3(e). Fig. 3(b) provides a schematic of the local cutting method.

To overcome the challenge that conventional abrasive grains often generate scratches too shallow for detailed morphological or mechanistic analysis, this study employed single-grit diamond tools, which offer superior hardness and wear resistance. The use of diamond tools increases scratch depth and enhances morphological contrast, enabling stable cutting conditions and accurate surface characterization. This approach facilitates clear elucidation of the material removal mechanisms. Four different rake angles (0°,  $-10^{\circ}$ ,  $-20^{\circ}$ , and  $-30^{\circ}$ ) were evaluated. For each rake angle, three lubrication modes—dry cutting, MQL, and NMQL—were implemented. The nano-lubricant was prepared by dispersing a mixture of 200 nm MoS<sub>2</sub> and 20 nm Fe<sub>3</sub>O<sub>4</sub> nanoparticles in a commercial oil using mechanical stirring and ultrasonic vibration. The mass ratio of MoS<sub>2</sub>/Fe<sub>3</sub>O<sub>4</sub> was set to 1:1, and the total nanoparticle mass fraction was 6 %. Scratch tests were conducted at a cutting speed of 1 m/min, a feed rate of 3 µm/rev, and a depth of cut that was progressively varied from 0 to 5  $\mu m$  per pass. Each combination of rake angle and lubrication mode was tested in duplicate to ensure the reliability and reproducibility of the data. For each individual scratch, the tool was engaged with the workpiece under the specified parameters; following a sustained cutting period, the tool was retracted in a controlled manner until the cutting force returned to zero prior to commencing the next test or repetition.

# 3.2. Experimental validation

Fig. 4 presents the experimental cutting force values for four rake angles under three lubrication modes in cylindrical grinding experiments. All tests were conducted at a spindle speed of 1 m/min, a depth of cut of 5  $\mu$ m, and a feed per revolution of 3  $\mu$ m/rev.

The results indicate that the combined effect of lubrication mode and

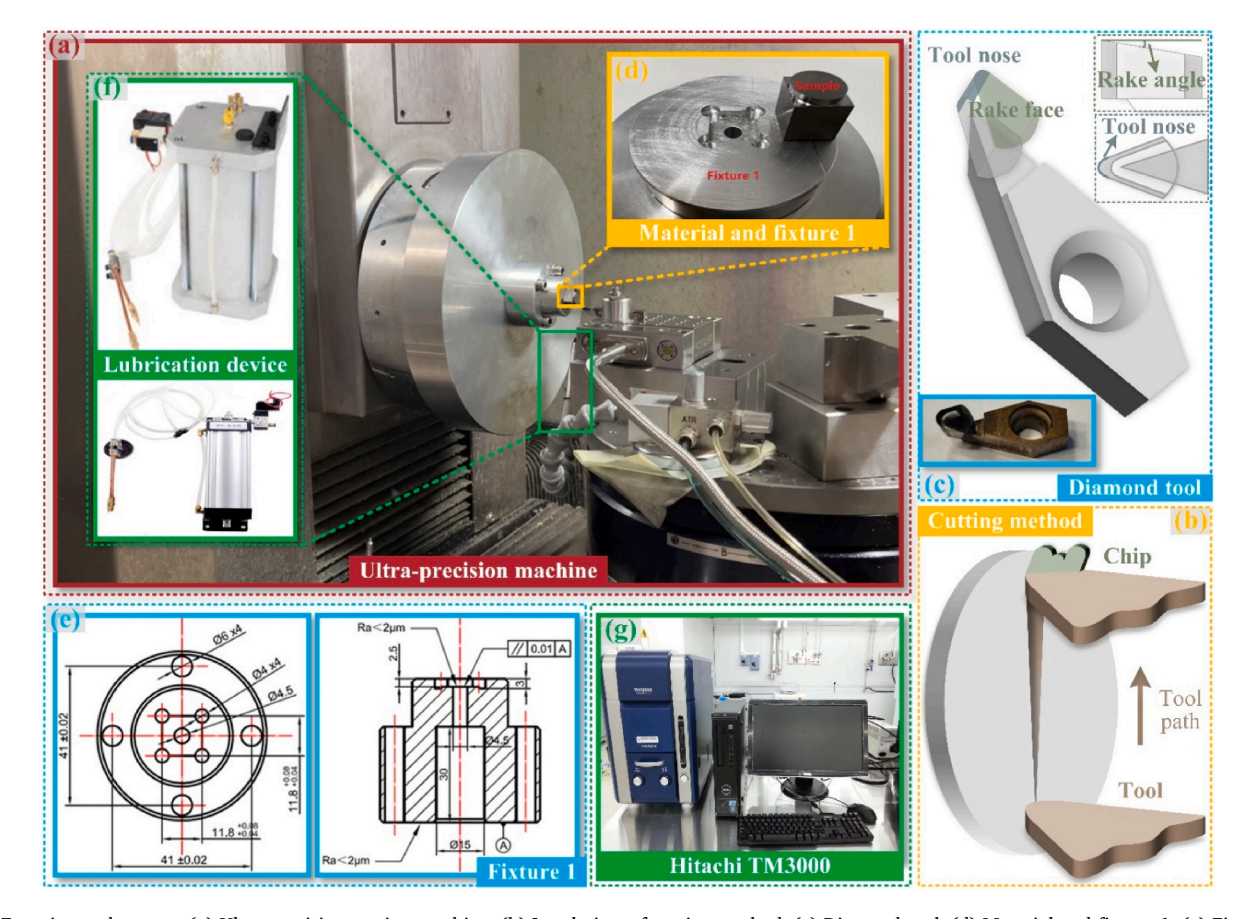


Fig. 3. Experimental system: (a) Ultra-precision cutting machine, (b) Local view of cutting method, (c) Diamond tool, (d) Material and fixture 1, (e) Fixture 1, (f) Lubrication device, (g) Field-emission SEM.

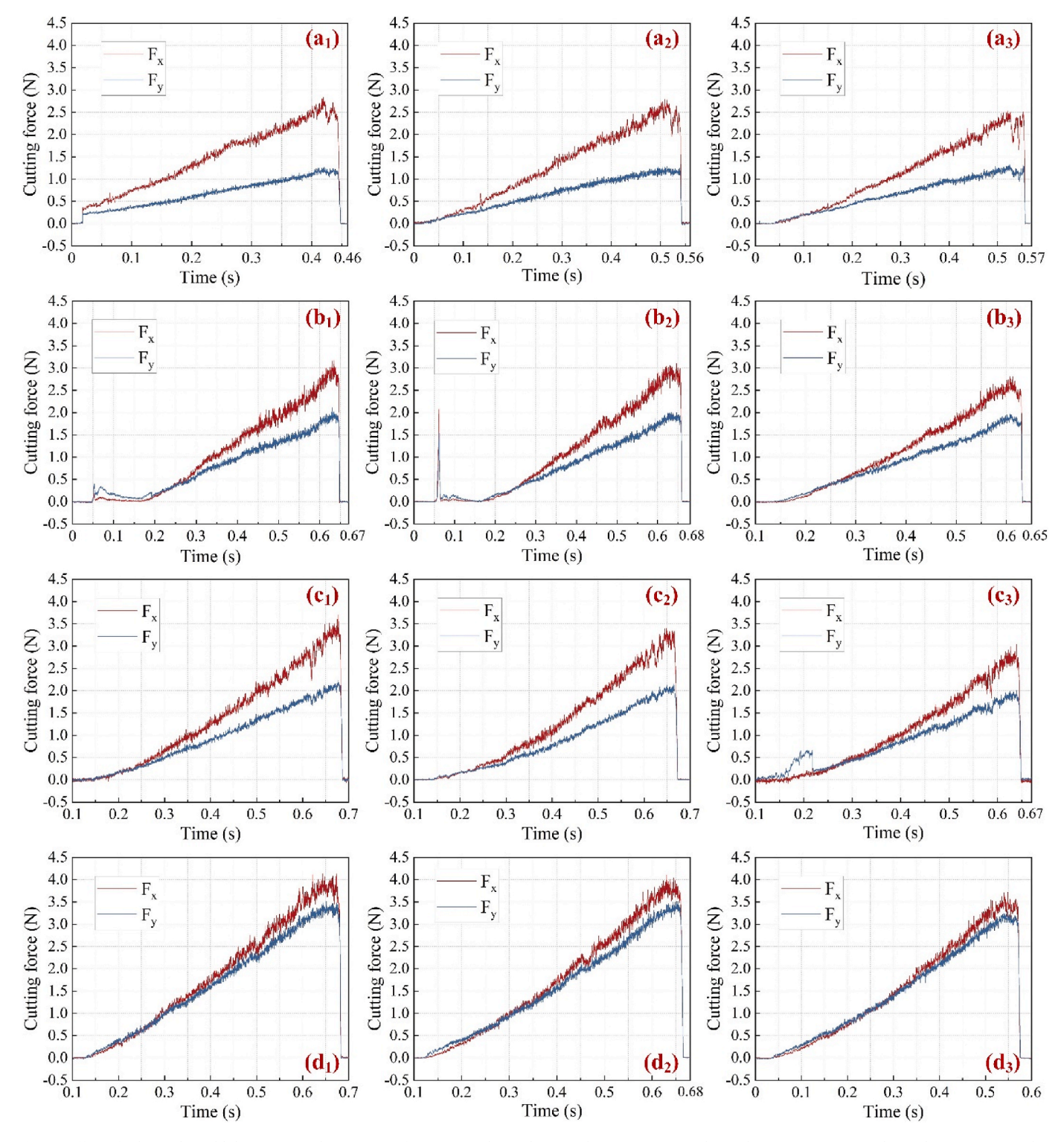


Fig. 4. Effect of rake angle and lubrication mode on cutting force:  $(a_1)$  Rake angle  $=0^\circ$ , dry cutting;  $(a_2)$  Rake angle  $=0^\circ$ , MQL;  $(a_3)$  Rake angle  $=0^\circ$ , NMQL;  $(b_1)$  Rake angle  $=-10^\circ$ , dry cutting;  $(b_2)$  Rake angle  $=-10^\circ$ , MQL;  $(b_3)$  Rake angle  $=-10^\circ$ , NMQL;  $(c_1)$  Rake angle  $=-20^\circ$ , dry cutting;  $(c_2)$  Rake angle  $=-20^\circ$ , MQL;  $(c_3)$  Rake angle  $=-20^\circ$ , NMQL;  $(d_1)$  Rake angle  $=-30^\circ$ , dry cutting;  $(d_2)$  Rake angle  $=-30^\circ$ , MQL;  $(d_3)$  Rake angle  $=-30^\circ$ , NMQL.

tool rake angle significantly affects cutting forces. Cutting forces increase with larger absolute values of negative rake angle. A more negative rake angle promotes the formation of thicker chips and increases the tool—workpiece contact area, making chip separation more difficult and causing a notable increase in cutting force. Lubrication mode critically influences this relationship. Under dry cutting, the effect of rake angle is amplified; decreasing the negativity of the rake angle

facilitates chip flow and reduces force through lower frictional dissipation. Conversely, under both MQL and NMQL conditions, the lubricant reduces friction between the chip and tool, thereby moderating the effect of rake angle. Nevertheless, the beneficial effect of increasing rake angle in reducing cutting force remains observable.

Additionally, as seen in Fig. 4, decreasing the rake angle reduces the difference between tangential force and normal force, which is primarily

attributable to changes in the material removal mechanism. At a rake angle of  $0^{\circ}$ , chip formation occurs mainly via plastic shear flow. At negative rake angles, chip formation is dominated by squeezing and plowing actions. With a more negative rake angle, tool penetration becomes more difficult, resulting in an increased normal force.

Fig. 5 compares experimental and simulated cutting force values for four rake angles under three lubrication modes, with all other parameters held constant. In Fig. 5(a), under dry cutting, the experimental tangential and normal forces for rake angles of  $0^\circ, -10^\circ, -20^\circ,$  and  $-30^\circ$  are 2.83 N and 1.33 N, 3.18 N and 2.12 N, 3.71 N and 2.24 N, and 4.15 N and 3.52 N, respectively. The minimum simulation error occurs at a rake

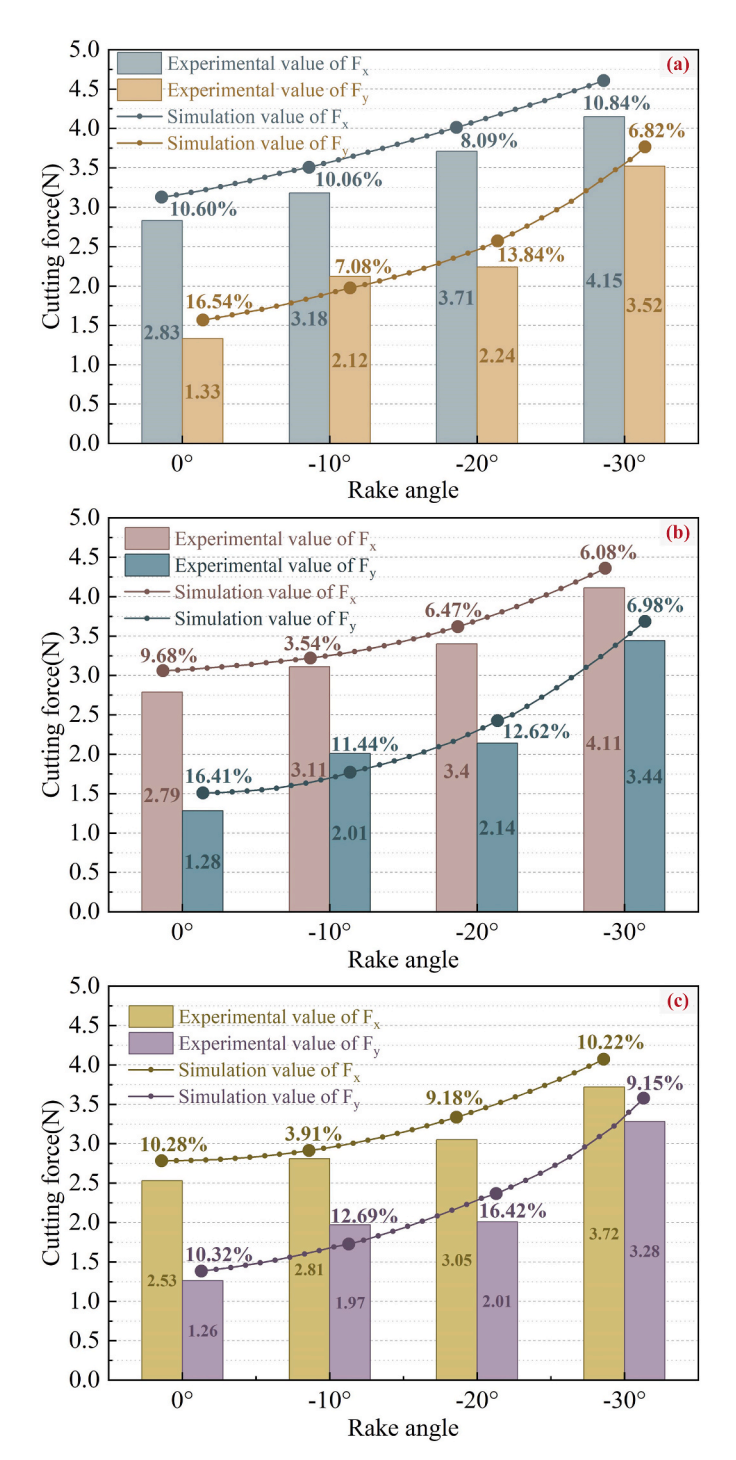


**Fig. 5.** Effect of rake angle and lubrication mode on cutting force: (a) Dry cutting; (b) MQL; (c) NMQL.

angle of  $-10^{\circ}$ , with a deviation of 6.13 % between the experimental and simulated normal forces. In Fig. 5(b), under MQL, the experimental tangential and normal forces for the same rake angles are 2.79 N and 1.28 N, 3.11 N and 2.01 N, 3.40 N and 2.14 N, and 4.11 N and 3.44 N, respectively. Here, the minimum simulation error is 3.54 % at  $-10^{\circ}$ . In Fig. 5(c), under NMQL, the corresponding forces are 2.53 N and 1.26 N, 2.81 N and 1.97 N, 3.05 N and 2.01 N, and 3.72 N and 3.28 N. Again, the minimum simulation error is 3.54 % at  $-10^{\circ}$ . Most predicted errors are approximately 10 %, indicating that the model exhibits satisfactory predictive accuracy. However, larger errors are observed in groups such as the 0° rake angle under dry cutting and MQL modes, which is mainly due to the small magnitude of the normal force—thus, small absolute deviations produce relatively large percentage errors. Furthermore, changes in lubrication mode may lead to deviations in the friction coefficient, and the Oxley model does not fully capture the non-uniform lubrication state.

As shown in Table 3, simulation errors remain within a reasonable range, with a relatively uniform distribution, demonstrating good applicability of the model for dry cutting. Nevertheless, some fluctuations and systematic deviations are present. In particular, under dry cutting at a rake angle of  $-30^{\circ}$ , the simulation error of the main cutting force reaches 0.45, the highest among all groups. This may be attributed to severe built-up edge formation; at  $-30^{\circ}$ , the tool-chip contact length increases and chip flow becomes unfavorable. The absence of lubrication under dry cutting facilitates material adhesion to the rake face, promoting built-up edge formation, which dramatically reduces the effective rake angle, increases resistance, and introduces instability in chip formation. It is also noteworthy that only at the rake angle of  $-10^{\circ}$ are the experimental values across all lubrication modes consistently lower than the simulation values, resulting in negative errors. This may reflect a transitional behavior in the plastic deformation mechanism of TC4; as the rake angle decreases from  $0^{\circ}$  to  $-10^{\circ}$ , the deformation mode shifts from uniform sliding to one dominated by local shear bands. This critical transition is not adequately represented by the simulation model, resulting in negative errors.

Fig. 6 displays the experimental and simulated cutting force values for four rake angles under different lubrication modes and varying friction coefficients, with all other parameters constant. As the friction coefficient increases, both the main cutting force and the normal force increase. In Fig. 6(a), a higher friction coefficient increases sliding resistance between the chip and tool, resulting in a higher main cutting force. In contrast, the growth rate of the normal force in Fig. 6(b) is lower, as it is mainly affected by the lateral plastic deformation of the workpiece and is less affected by the friction coefficient.

## 3.3. Scratch depth and chip formation

Scratch morphology provides a direct visual observation of the microscopic interaction processes between the tool and workpiece, revealing the material removal method, crack propagation, and adhesion state. This facilitates a mechanistic understanding of tool wear and cutting behavior during the grinding of titanium alloys, particularly regarding the evolution of scratch characteristics under different rake angles and friction conditions. As shown in Fig. 7, the scratch morphologies illustrate typical surface features formed by diamond tools on TC4 under different rake angles and lubrication modes. The six scratches, progressing from left to right, correspond to dry cutting, MQL,

**Table 3**Simulation error under different lubrication modes and rake angles.

	<b>0</b> °		_10°		$-20^{\circ}$		$-30^{\circ}$	
	$F_x$	$F_y$	$F_x$	$F_y$	$F_x$	$F_y$	$F_x$	Fy
Dry Cutting MQL NMQL	0.30 0.27 0.26	0.22 0.21 0.13	0.32 0.11 0.11	-0.15 $-0.23$ $-0.25$	0.30 0.22 0.28	0.31 0.27 0.33	0.45 0.25 0.38	0.24 0.24 0.3

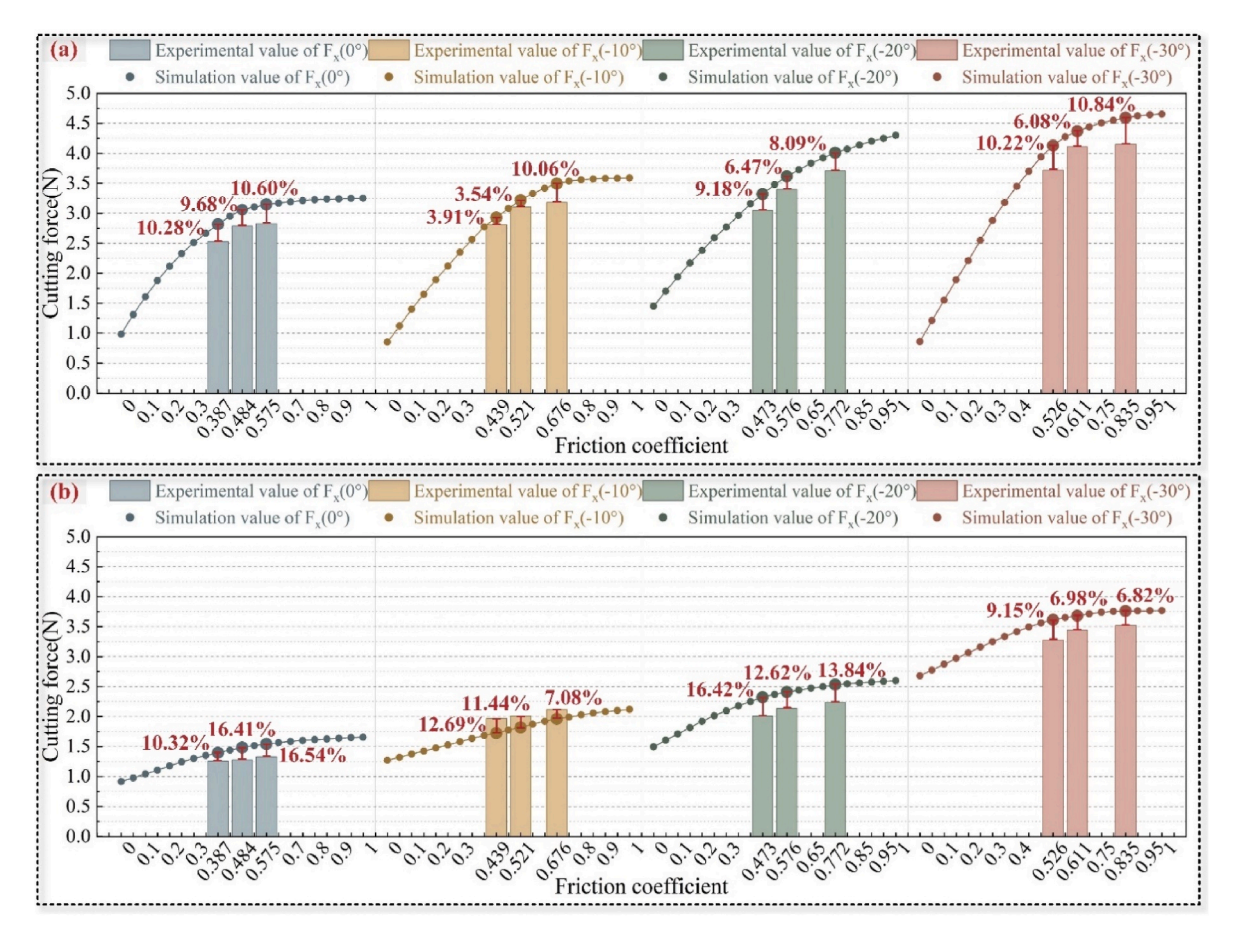


Fig. 6. Effect of lubrication modes on cutting force: (a) F<sub>x</sub>, (b) F<sub>y</sub>.

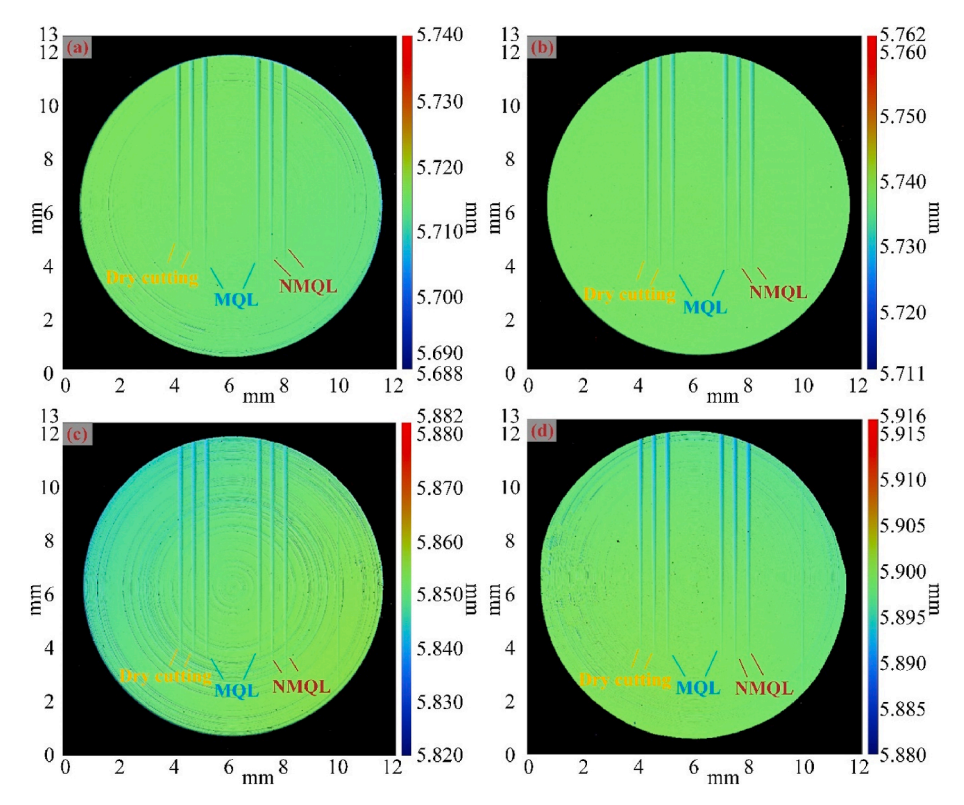
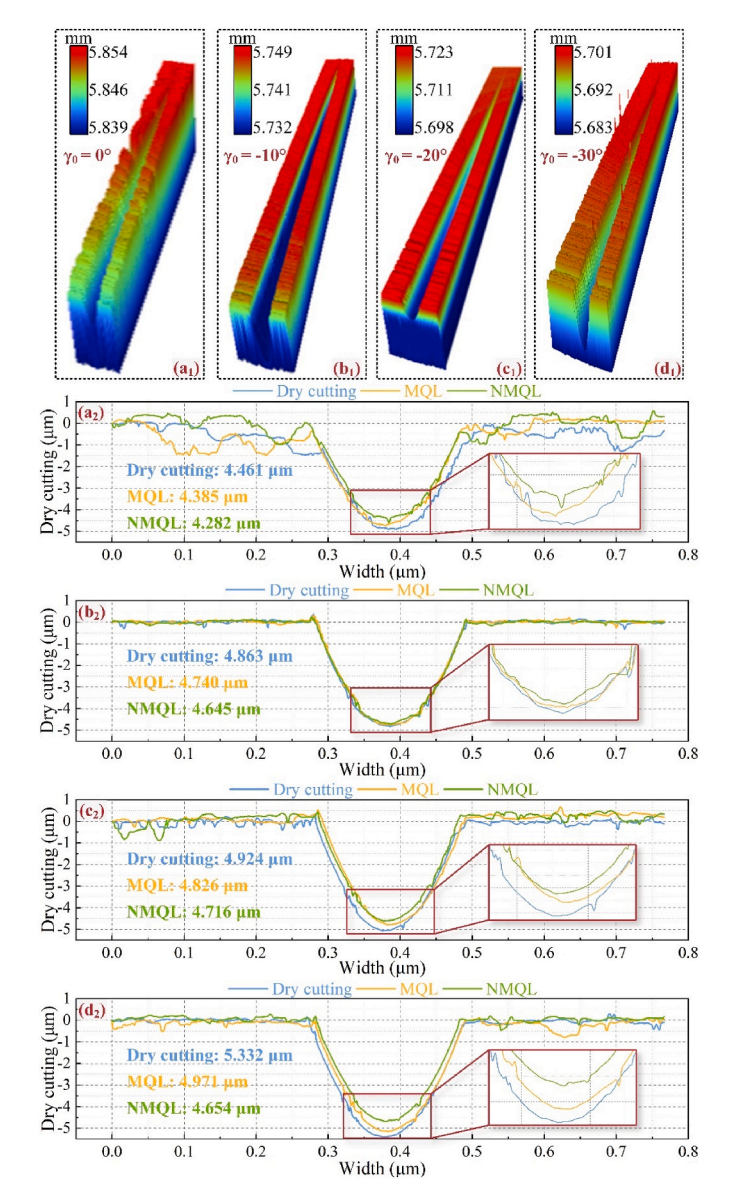


Fig. 7. Scratch morphologies under four rake angles: (a)  $0^{\circ}$ , (b)  $-10^{\circ}$ , (c)  $-20^{\circ}$ , and (d)  $-30^{\circ}$ .

and NMQL, with two scratches for each lubrication condition. The scratch morphologies clearly demonstrate the significant effect of lubrication mode on surface quality. Under dry cutting, substantial heat accumulation occurs, leading to a higher propensity for surface damage. MQL mode offers notable improvement compared with dry cutting; however, insufficient lubrication persists in high-load regions. NMQL further enhances lubrication and cooling, as the presence of nanoparticles suppresses irregular scratches and material tearing. Rake angle also plays a key role: decreasing rake angle increases both cutting force and heat accumulation, leading to localized damage and elevated surface roughness.

Fig. 8 presents three-dimensional scratch morphologies under NMQL at different rake angles. A clear progression is observed: at a rake angle of  $0^{\circ}$  (Fig. 8(a<sub>1</sub>)), the scratch appears shallow, narrow, and uniform, indicative of a shearing-dominated cutting process. Material is removed efficiently with low resistance, and NMQL further reduces friction and heat, resulting in high surface integrity with minimal bulging or tearing along the scratch edges. At rake angles of  $-10^{\circ}$  and  $-20^{\circ}$  (Fig. 8(b<sub>1</sub>), (c<sub>1</sub>)), the increased contact angle restricts chip flow, causing a shift from



**Fig. 8.** Scratch morphologies under NMQL mode at four rake angles: (a<sub>1</sub>)  $0^{\circ}$ , (b<sub>1</sub>)  $-10^{\circ}$ , (c<sub>1</sub>)  $-20^{\circ}$ , and (d<sub>1</sub>)  $-30^{\circ}$ , and scratch depth under three lubrication modes at four rake angles: (a<sub>2</sub>)  $0^{\circ}$ , (b<sub>2</sub>)  $-10^{\circ}$ , (c<sub>2</sub>)  $-20^{\circ}$ , and (d<sub>2</sub>)  $-30^{\circ}$ .

pure shearing to a combination of shearing and plowing. Localized groove deepening and edge bulging are more prominent, and the material experiences increased compressive and shear stresses, resulting in plastic accumulation ahead of the tool and lateral flow. At  $-30^{\circ}$  (Fig. 8 (d<sub>1</sub>)), the removal mechanism is dominated by severe plowing, microfracture, and localized tearing; chip flow is significantly hindered, and the resulting morphology is characterized by discontinuous, rough, and fragmented traces. Such features indicate intense plastic strain, potential microcrack initiation, and even brittle delamination within the deformed layer. Although NMQL helps reduce interfacial friction and temperature, the pronounced mechanical interaction associated with the aggressive negative rake geometry dominates, leading to aggravated surface damage and reduced surface quality.

Fig. 8 also displays the cross-sectional profiles of scratches across four rake angles and three lubrication modes. Scratch depth increases as rake angle decreases. Under dry cutting, the maximum scratch depth rises from 4.461  $\mu m$  at  $0^{\circ}$  to 5.332  $\mu m$  at  $-30^{\circ}$ , an increase of approximately 19.5 %. This is attributed to the effective bluntness of the tool edge at more negative rake angles, which shifts the material removal mechanism from shear-dominated to extrusion-dominated. This transition results in more severe plastic deformation and material pile-up, vielding deeper scratches. Lubrication mode also has a substantial effect. At a given rake angle, scratch depth decreases progressively from dry cutting to MQL to NMQL. For example, at 0°, scratch depth under NMQL is  $4.282 \mu m$ – $0.179 \mu m$  less than under dry cutting. This reduction is due to the enhanced lubricating effect of the nanofluid in NMQL, as nanoparticles fill micro-grooves and form a stable lubricating film at the tool-chip interface. The film reduces friction and cutting temperature, suppresses material adhesion and extrusion, and ultimately leads to a shallower, more refined scratch morphology.

Scratch morphology reflects the plastic flow and damage evolution on the titanium alloy surface at the micro- and nano-scale. In parallel, chip morphology analysis provides insight into the dynamic shear characteristics and energy dissipation during macroscopic material removal. Fig. 9 presents chip morphologies at different rake angles under dry cutting. At 0° (Fig. 9(a<sub>1</sub>), (a<sub>2</sub>)), chips are spiral, with small curvature and moderate bending; the chip edge is smooth, shear bands are clear and continuous, surface quality is high, and deformation is uniform, indicating a well-developed shear slip layer. At  $-10^{\circ}$  (Fig. 9 (b<sub>1</sub>), (b<sub>2</sub>)), chip curling increases markedly, and deformation intensifies. Local adhesions and discontinuous edge marks appear, reflecting that decreasing rake angle increases the shear surface angle, causing the material to adhere and separate incompletely, resulting in rough chip edges and fluctuations in the slip layer. At  $-20^{\circ}$  (Fig. 9(c<sub>1</sub>), (c<sub>2</sub>)), chip curvature further increases, chips become tightly curled, and obvious non-smooth structures appear at the edge. Enlarged images reveal dense, disordered slip lines; the material in the slip layer is more intensely deformed, but instability increases. At  $-30^{\circ}$  (Fig. 9(d<sub>1</sub>), (d<sub>2</sub>)), chips are severely curled, curvature is maximal, and clear brittle fracture occurs locally. The edge is rough and discontinuous, and obvious adhesion and tearing marks are present in several regions. At this rake angle, the cutting process is highly unstable, tool loading is significant, and surface quality is further compromised, with an increased risk of tool damage.

# 4. Results analysis and discussion

The material removal mechanism in ultra-precision cutting of TC4 titanium alloy is predominantly controlled by the synergistic effects of tool rake angle and lubrication mode, as quantitatively demonstrated through chip morphology evolution and thermomechanical analysis of the shear zone (Fig. 10). Under dry cutting conditions, elevated interfacial friction promotes severe adiabatic shear localization, resulting in chaotic shear bands with irregular spacing and blocky chip segments. This instability is attributed to excessive heat accumulation, which accelerates crater wear via Ti–6Al–4V adhesion and diffusion, and leads to

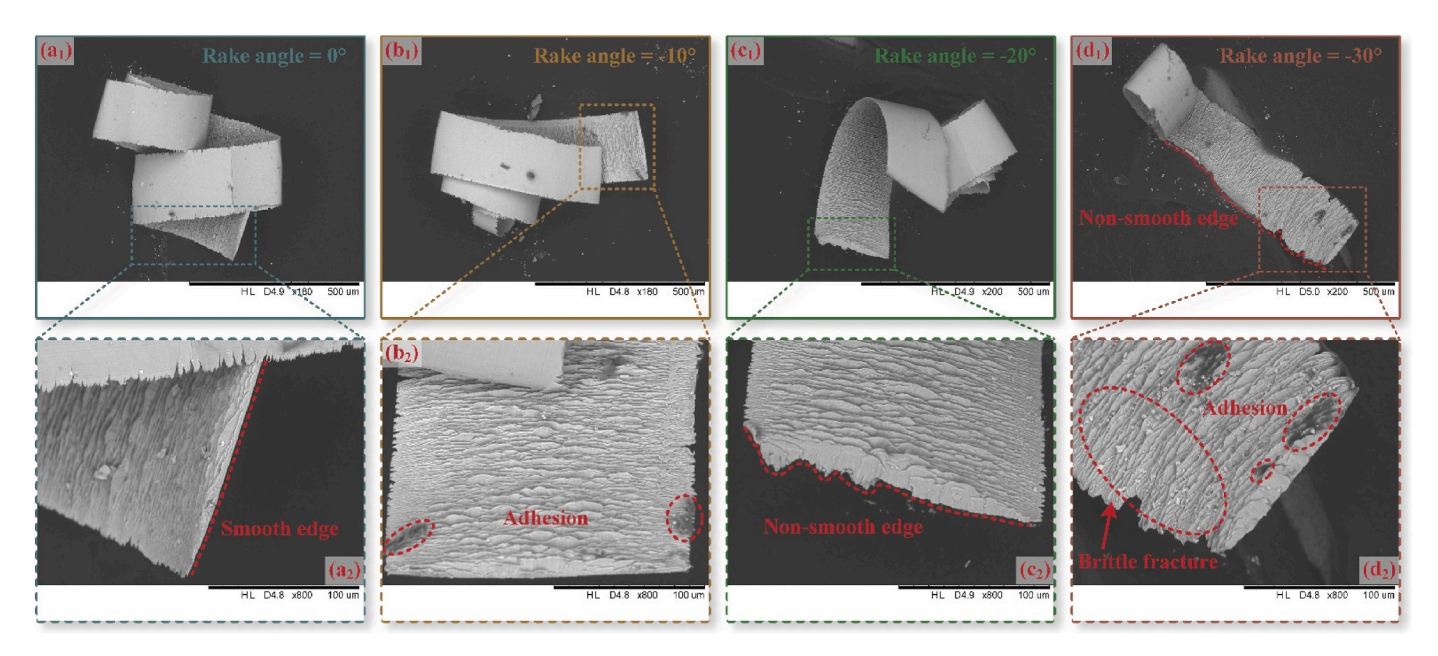


Fig. 9. Chip morphologies at four rake angles:  $(a_1) \ 0^\circ$ ,  $(b_1) \ -10^\circ$ ,  $(c_1) \ -20^\circ$ ,  $(d_1) \ -30^\circ$  and corresponding magnified views  $(a_2) \ 0^\circ$ ,  $(b_2) \ -10^\circ$ ,  $(c_2) \ -20^\circ$ ,  $(d_2) \ -30^\circ$ .

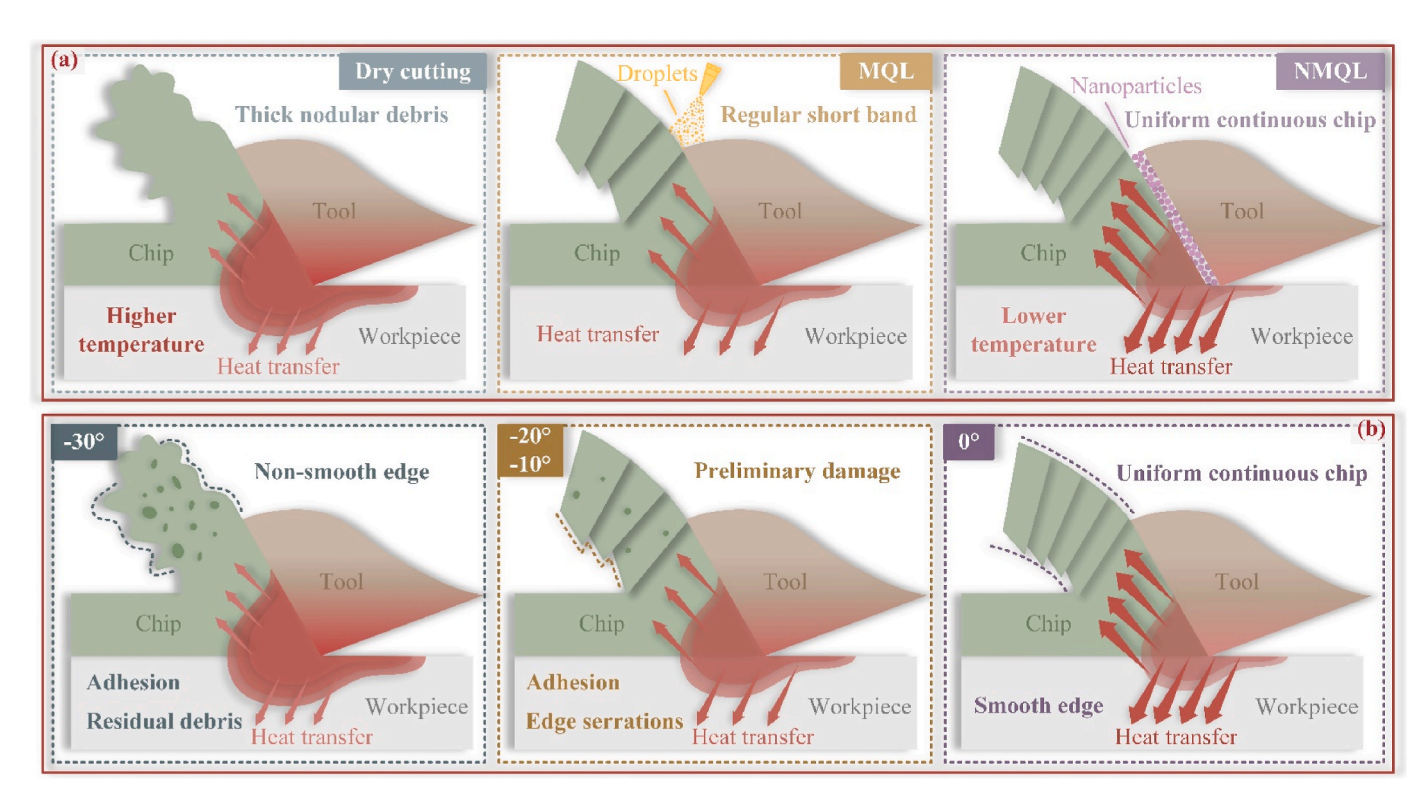


Fig. 10. Analysis of (a) lubrication mode and (b) rake angle.

rapid progression of flank wear. This observation is consistent with the findings of Gupta et al. [52] on carbide tool wear during Ti–6Al–4V machining. Sarma et al. [53] investigated the machinability of Ti–6Al–4V alloy under MQL conditions, revealing that MQL reduces the friction angle and lowers shear stress through oil-mist penetration at the tool-chip interface. The improved heat dissipation supports the formation of periodic adiabatic shear bands and the production of short, curled chips with controlled curvature radii, indicating stabilized plastic flow.

Expanding on this foundation, the present study investigates the effects of NMQL. The addition of nanoparticles facilitates the formation of

a tribo-film, which further reduces friction, shortens the sticking zone length, and narrows shear band spacing. These changes enable the formation of continuous, thin-band chips with nearly uniform curvature, signifying a transition to quasi-steady-state shear.

Simultaneously, the rake angle plays a critical role in modulating shear mechanics and chip formation. Previous studies by Wu and To Ref. [54] investigated rake angles of  $0^\circ,\ 10^\circ,\$ and  $20^\circ,\$ without addressing negative rake angles. Li et al. [55] analyzed chip formation over a range from  $-15^\circ$  to  $15^\circ.$  Building on these works, the present study extends the analysis to include negative rake angles down to  $-30^\circ.$  Extreme negative geometry ( $\gamma=-30^\circ)$  significantly increases

compressive stress, raising frictional work and producing thick, nodular debris with fragmented lamellae, ultimately degrading surface integrity. In contrast, a neutral rake angle ( $\gamma=0^\circ$ ) optimizes shear plane orientation, minimizing shear stress and enabling the formation of stable ribbon chips with smooth edges and minimal subsurface damage. The observed transition from unstable fracture (dry cutting,  $\gamma=-30^\circ$ ) to controlled shear (NMQL,  $\gamma=0^\circ$ ) highlights the critical influence of interfacial tribology on precision removal efficiency in titanium alloy machining.

#### 5. Conclusions

This study investigates the material removal mechanism and cutting force behavior during diamond tool grinding of TC4 titanium alloy, focusing on the effects of rake angle and lubrication mode. The findings provide guidance for optimizing cutting parameters for TC4. The main conclusions are as follows.

- (i) By integrating friction effects, thermal-force coupling, and stress-strain evolution, a predictive model was established based on the classical Oxley shear model and the Johnson-Cook constitutive equation. The influence of various rake angles on cutting force and material removal during ultra-precision machining with diamond tools was systematically investigated.
- (ii) Experimental validation confirmed the model's reliability, with a minimum prediction error of 3.54 % and an average error of 8.23 %. The predicted cutting force values exhibited strong agreement with experimental results, and the overall trends were consistent between theoretical and experimental data.
- (iii) During grinding of TC4 titanium alloy, smaller rake angles increase both the depth of scratch and the extent of chip deformation, with material removal dominated by plowing and brittle fracture. As the lubrication mode transitions from dry to MQL and then to NMQL, the scratch depth decreases accordingly. Rake angle and lubrication mode together modulate the material removal mechanism, thereby controlling surface quality in ultraprecision machining.

This study demonstrates notable progress in ultra-precision machining through the application of NMQL. Nonetheless, several key areas merit further investigation: (a) Advancing lubrication and cooling technologies remains a critical topic. The development of new nanolubricants with low friction coefficients and high thermal conductivity may further enhance processing quality. (b) Continued improvement in tool design and surface modification is necessary. The use of topology optimization algorithms is proposed as a promising research direction to reduce cutting force fluctuations and improve chip control.

#### Declaration of competing interest

The authors declare that they have no known competing financial interests or personal relationships that could have appeared to influence the work reported in this paper.

## Acknowledgments

This research was financially supported by the following organizations: the National Natural Science Foundation of China (No. 52475469, 52375447), the Shandong Provincial Natural Science Foundation, China (ZR2024ME255, ZR2024QE100), and the Special Fund of Taishan Scholars Project (No. tsqn202211179).

#### References

[1] Cui X, Li C, Ding W, Chen Y, Mao C, Xu X, Liu B, Wang D, Li HN, Zhang Y, Said Z, Debnath S, Jamil M, Ali HM, Sharma S. Minimum quantity lubrication machining

- of aeronautical materials using carbon group nanolubricant: from mechanisms to application. Chin J Aeronaut 2022;35(11):85–112.
- [2] Su J, Jiang F, Teng J, Chen L, Yan M, Requena G, Zhang L-C, Wang YM, Okulov IV, Zhu H, Tan C. Recent innovations in laser additive manufacturing of titanium alloys. Int J Extrem Manuf 2024;6(3).
- [3] Wang Z, Liu J, Wang Y, Sun H, Yu H. The influence of interface morphology on the interfacial bonding behavior and mechanical properties of TC4/TA2 composite plates. Mater Sci Eng, A 2025;936:148401.
- [4] Jia Y, Lai J, Yu J, Qi H, Zhang Y, He H. Tribological behaviors of electroless nickel-boron coating on titanium alloy surface. Chin J Mech Eng 2024;37(1):13.
- [5] Gong P, Zhang Y, Cui X, Xu S, Yang M, Jia D, Li C. Lubricant transportation mechanism and wear resistance of different arrangement textured turning tools. Tribol Int 2024;196:109704.
- [6] Lal B, Wani MF, Dey A, Singh A. In-vitro analysis of TC4 alloy reinforced with inert ceramics for biomedical applications synthesized using spark plasma sintering. Tribol Int 2025;210:110744.
- [7] Yin J, Zhang C, Sun R, Hu Y, Miao Y, Li Y. Controllable kilohertz impact fatigue loading functioned by cyclic stress wave of Hopkinson tension bar and its application for TC4 titanium alloy. Int J Fatig 2025;194:108828.
- [8] Chen M, Yi Z, Xiong H, Zou H, Kang X, Zhang L, Zou J, Zhou K. Efficient catalytic debinding feedstock design for material extrusion additive manufacturing of low warpage and high-density titanium alloy. Appl Mater Today 2024;40:102383.
- [9] Zhang S, Wang D, Zhao F, Zhang Z, Zhou H, Chen L, Yan L, Zhao B. Close atomic surface of titanium alloy produced by novel photocatalytic chemical mechanical polishing using developed SiO2@Al2O3@CeO2 composite abrasives with high material removal rate. Appl Surf Sci 2025;703:163436.
- [10] Li H, Zou L, Gui L, Li Y, Zhang X, Wang W. Effects of feed direction on material removal behavior in belt grinding of titanium alloys. J Manuf Process 2023;102: 756–64
- [11] Pei W, Xie Z, Wang J, Pei X, Zhang Q, Liu J. Tribocorrosion performance of TC4 anodized/carbon fiber composite in marine environment. J Mater Res Technol 2024;32:762–73.
- [12] An QYJ, Li J, Liu G, Chen M, Li C. A state-of-the-art review on the intelligent tool holders in machining. Intell Sustain Manuf 2024;1:10002.
- [13] Biyik S, Arslan F, Aydin M. Arc-erosion behavior of boric oxide-reinforced silver-based electrical contact materials produced by mechanical alloying. J Electron Mater 2014;44(1):457–66.
- [14] Biyik S, Aydin M. A new life-test equipment designed for medium-duty electromagnetic contactors. In: Proceedings of the 2014 15th international conference on thermal, mechanical and multiphysics simulation and experiments in microelectronics and microsystems (EuroSimE); 2014. Belgium.
- [15] Xu D, Ai T, Shen Z, Ma S, Hossen MS, Liao Z. Materials removal mechanism in laser-assisted grinding of SiC fibre-reinforced titanium alloy composite. CIRP Annals 2025.
- [16] Wang M, Qu N. Investigation on material removal mechanism in mechanoelectrochemical milling of TC4 titanium alloy. J Mater Process Technol 2021;295: 117206.
- [17] Siva Surya M. Optimization of turning parameters while turning Ti-6Al-4V titanium alloy for surface roughness and material removal rate using response surface methodology. Mater Today Proc 2022;62:3479–84.
- [18] An Q, Yang J, Li J, Liu G, Chen M, Li CJI, Manufacturing S. A state-of-the-art review on the intelligent tool holders in machining 2024;1(1):10002.
- [19] Gu G, Wang D, Wu S, Zhou S, Zhang BJI, Manufacturing S. Research status and prospect of ultrasonic vibration and minimum quantity lubrication processing of nickel-based alloys 2024;1(1):10006.
- [20] Zhao L, Zhang J, Zhang J, Dai H, Hartmaier A, Sun T. Numerical simulation of materials-oriented ultra-precision diamond cutting: review and outlook, 5; 2023, 022001 2.
- [21] Cui X, Li C, Yang M, Liu M, Gao T, Wang X, Said Z, Sharma S, Zhang Y. Enhanced grindability and mechanism in the magnetic traction nanolubricant grinding of Ti-6Al-4 V. Tribol Int 2023:186:108603.
- [22] Wang H, Bai Q, Chen S, Wang P, Guo W, Dou Y. Wear suppression and interface properties of diamond tool in micro-milling of TC4 alloy under graphene nanofluid MQL environment. J Clean Prod 2023;418:138180.
- [23] Dong D, Zhang J, Chen K, Wu Z, Zhang X, Cui J, Zeng L. Influence of sintering temperature on micro morphology and mechanical properties of CNTs/TC4 composites prepared by electromagnetic impacting. Ceram Int 2025.
- [24] Duan Z, Wang Z, Wang S, Zhang B, Bian P, Li Y, Liu J, Song J, Li C, Liu X. Tool wear in enhanced minimum quantity lubrication assisted milling: from mechanism to application. Chin J Aeronaut 2025:103597.
- [25] Sun CHP, Hu Z, Liang X. Metallurgical characteristics of 316L stainless steel by laser additive manufacturing. Intell Sustain Manuf 2024;1:10012.
- [26] Ma J, Zhang Y, Li Y, Shan C, Jiao F, Gao G, Zhang D, Zhao B. Cutting force prediction model considering tool-chip contact interface friction behavior in ULTVAM of Ti-6Al-4V. Chin J Aeronaut 2025;38(6):103212.
- [27] Shen X, Zhang D, Yao C, Tan L, Li X. Research on parameter identification of Johnson–Cook constitutive model for TC17 titanium alloy cutting simulation. Mater Today Commun 2022;31:103772.
- [28] Li S, Zhang D, Liu C, Shao Z, Ren L. Influence of dynamic angles and cutting strain on chip morphology and cutting forces during titanium alloy Ti-6Al-4 V vibrationassisted drilling. J Mater Process Technol 2021;288:116898.
- [29] Kaynak Y, Ozkutuk M, Kitay O. Numerical simulation of cutting-induced grain refinement in machining process under dry and MQL conditions of titanium Ti-5553 alloy. Proced CIRP 2025;133:716–21.
- [30] Siahsarani A, Alinaghizadeh A, Azarhoushang B, Bayat M, Bösinger R. Sustainable and efficient cooling in titanium milling for dental applications: a study on

- supercritical CO2 + MQL with focus on tool wear and surface topography. Wear 2025:572-3, 206051.
- [31] Li M, Li Q, Pan X, Wang J, Wang Z, Xu S, Zhou Y, Ma L, Yu T. On understanding milling characteristics of TC4 alloy during graphene nanofluid minimum quantity lubrication with bionic micro-texture tool. J Mater Res Technol 2025;36:4200–14.
- [32] Chen MZY, Liu B, Zhou Z, Zhang N, Wang H. Design of intelligent and sustainable manufacturing production line for automobile wheel Hu. Intell Sustain Manuf 2024;1:10003.
- [33] Mohandas, Hosamani B, Nagaraju, Kemminje V, Raju VR, Nagahanumaiah. An investigation into the surface integrity and cutting force characteristics in titanium alloy end milling using soluble oil and MQL as coolants. Results Surf Interfaces 2024;17:100341.
- [34] Shi L, Yin Y, Wang C, Wang T, Yang L, Wang Q, An Q, Ming W, Chen M. Study on the effects of scCO2 cooling and MQL conditions on the milling machinability of titanium alloys. Wear 2025;576–577:206036.
- [35] Sarma D, Ozah R, Chandrasekaran M, Sahoo AK, Kumar R, Pattanayak S. Material-specific machining optimization of Ti6Al4V alloy under MQL: a sustainability-centric approach. Next Mater 2025;8:100586.
- [36] Sen B, Bhowmik A. Application of minimum quantity GnP nanofluid and cryogenic LN2 in the machining of Hastelloy C276. Tribol Int 2024;194:109509.
- [37] Chetan Ghosh S, Rao PV. Comparison between sustainable cryogenic techniques and nano-MQL cooling mode in turning of nickel-based alloy. J Clean Prod 2019; 231:1036–49.
- [38] Li W, Zeng Z, Le S, Zhu K, Huang X, Hegab H, Ibrahim AMM. Investigation of a green nanofluid added with graphene and Al2O3 nano-additives for grinding hard-to-cut materials. Tribol Int 2024;195:109580.
- [39] Liu CZY, Zhu L, Li Q, Shu X, Qin S. A review of ultrasonic vibration-assisted grinding for advanced materials. Intell Sustain Manuf 2025;2:10001.
- [40] Biyik S. Effect of Y2O3 addition and milling time on the synthesis of nanocrystalline Ag–ZnO composite powder via mechanical alloying. J Radiat Res Appl Sci 2024;17(2):100867.
- [41] Biyik S. Characterization of nanocrystalline Cu25Mo electrical contact material synthesized via ball milling. Acta Phys Pol, A 2017;132(3-II):886–8.
- [42] Kim W-Y, Senguttuvan S, Kim SH, Lee SW, Kim S-M. Numerical study of flow and thermal characteristics in titanium alloy milling with hybrid nanofluid minimum quantity lubrication and cryogenic nitrogen cooling. Int J Heat Mass Tran 2021; 170:121005.
- [43] Namlu RH, Lotfi B, Kılıç SE. Enhancing machining efficiency of Ti-6Al-4V through multi-axial ultrasonic vibration-assisted machining and hybrid nanofluid minimum quantity lubrication. J Manuf Process 2024;119:348–71.

- [44] Pan Z, Shih DS, Tabei A, Garmestani H, Liang SY. Modeling of Ti-6Al-4V machining force considering material microstructure evolution. Int J Adv Des Manuf Technol 2017;91(5–8):2673–80.
- [45] Zhang Y, Gong P, Tang L, Cui X, Jia D, Gao T, Dambatta YS, Li C. Topography modeling of surface grinding based on random abrasives and performance evaluation. Chin J Mech Eng 2024;37(1):93.
- [46] Seif CY, Hage IS, Hamade RF. Incorporating dual BCC/FCC Zerilli-Armstrong and blue brittleness constitutive material models into Oxley's machining shear zone theory. J Manuf Process 2020;50:663–75.
- [47] Shu A, Zhou J, Ren J, Wang Z. A modified constitutive model considering dynamic recrystallization behavior for cutting Inconel 718. J Manuf Process 2023;104: 189–204.
- [48] Liu D, Li C, Xu P, Wang W, Zhang Y, Yang M, Cui X, Li B, Liu M, Gao T, Suleiman Dambatta Y, Qin A. SiCp/Al composites from conventional to empowered machining: mechanisms and processability. Compos Struct 2024;346:118433.
- [49] Liu D, Li C, Dong L, Qin A, Zhang Y, Yang M, Gao T, Wang X, Liu M, Cui X, Ali HM, Sharma S. Kinematics and improved surface roughness model in milling. Int J Adv Des Manuf Technol 2024;131(5):2087–108.
- [50] Jiang H, Ren Z, Zou Z, Yuan S, Yi Y. Reinforcement effect of cutting process on machined surface quality and performance of aviation aluminum alloy 7075 based on Oxley-Welsh theory. J Manuf Process 2023;95:38–52.
- [51] Liang X, Liu Z, Wang B, Song Q, Cai Y, Wan Y. Prediction of residual stress with multi-physics model for orthogonal cutting Ti-6Al-4V under various tool wear morphologies. J Mater Process Technol 2021;288:116908.
- [52] Gupta MK, Korkmaz ME, Sarıkaya M, Krolczyk GM, Günay M. In-process detection of cutting forces and cutting temperature signals in cryogenic assisted turning of titanium alloys: an analytical approach and experimental study. Mech Syst Signal Process 2022:169.
- [53] Sarma D, Ozah R, Borah J, Chandrasekaran M, Sahoo AK. Intelligent machine learning strategies for minimizing machining power in minimum quantity lubrication machining of Ti6Al4V alloy. J Mater Eng Perform 2025.
- [54] Wu H, To S. Serrated chip formation and their adiabatic analysis by using the constitutive model of titanium alloy in high speed cutting. J Alloys Compd 2015; 629:368–73.
- [55] Li A, Zang J, Zhao J. Effect of cutting parameters and tool rake angle on the chip formation and adiabatic shear characteristics in machining Ti-6Al-4V titanium alloy. Int J Adv Des Manuf Technol 2020;107(7–8):3077–91.